INORGANIC CHEMISTRY
FRONTIERS

PAPER

View Article Online
View Journal

Cite this: DOI: 10.1039/c3qi00103b

Oxidovanadium(IV), oxidomolybdenum(VI) and cobalt(III) complexes of *o*-phenylenediamine derivatives: oxidative dehydrogenation and photoluminescence†

Satyabrata Chaudhuri,[a] Sachinath Bera,[a] Manas Kumar Biswas,[a] Amit Saha Roy,[a] Thomas Weyhermüller[b] and Prasanta Ghosh*[a]

Reactions of *o*-phenylenediamine derivatives (L_3H_2) incorporating a (Ph)(Py)(H)C–N(H)– function with the oxidovanadium(IV) and oxidomolybdenum(VI) ions afford amide complexes of types $[V^{IV}O(L_3^{2-})]$ (**3**), $[V^{IV}O(L_3^{t\text{-}Bu\ 2-})]$ (**4**) and *cis*-$[Mo^{VI}O_2(L_3^{2-})]$ (**5**) (L_3H_2 = ((*E*)-2-(((2-((phenyl(pyridin-2-yl)methyl)amino)phenyl)imino)methyl)phenol); $L_3^{t\text{-}Bu}H$ = ((*E*)-2,4-di-*tert*-butyl-6-(((2-((phenyl(pyridin-2-yl)methyl)amino)phenyl)imino)methyl)phenol)), while the similar reaction of L_3H_2 with the anhydrous $CoCl_2$ in air results in oxidative dehydrogenation (OD) of the (Ph)(Py)(H)C–N(H)– function, affording a cobalt(III) diimine complex, *trans*-$[Co^{III}(L_4^-)Cl_2]$ (**6**) (L_4H = 2-((*E*)-(2-((*E*)-phenyl(pyridin-2-yl)methyleneamino)phenylimino) methyl)-phenol), contradicting the participation of the higher oxidation states of the metal ions in OD reaction of amines. **3–6** are characterized by elemental analyses and mass, IR, ^{1}H NMR and EPR spectra. The molecular geometries of **4**·CH_3OH, **5** and **6** were confirmed by single crystal X-ray structure determinations. The $V^{IV}–O_{phenolato}$ *cis* to the V=O bond and the V^{IV}=O lengths in **4**·CH_3OH are 1.925(2) and 1.612(2) Å. Two cis Mo=O lengths are 1.710(2) Å and 1.720(2) Å in **5**. The aliphatic –C–N– lengths in **4**·CH_3OH and **5** are 1.448(3) and 1.479(2) Å, while the same is 1.285(4) Å in **6**. DFT calculations on **3** and **6** inferred a significant mixing among d_M and NN-ligand backbone favoring a t_2^6 state of the metal ion for the OD of the amine fragment to have stronger $d_M \rightarrow \pi_{ketimine}^*$ back-bonding. The $\pi_{NHPh} \rightarrow \pi_{aldimine}^*$ transition of L_3H_2 is red shifted in **3** and **4** quenching the emissive $\pi_{Phenolato} \rightarrow \pi_{aldimine}^*$ transitions, elucidated by the TD DFT calculations on **3** (and $\mathbf{3}^+$). The $\pi_{NPh} \rightarrow \pi_{aldimine}^*$ transitions are blue shifted in the oxidovanadium(V) analogues, $[V^VO(L_3^{2-})]^+$ ($\mathbf{3}^+$) and $[V^VO(L_3^{t\text{-}Bu\ 2-})]^+$ ($\mathbf{4}^+$), which are fluorescent ($\mathbf{3}^+$, λ_{ex} = 331, λ_{em} = 444 nm; $\mathbf{4}^+$, λ_{ex} = 339, λ_{em} = 490 nm) recorded by the fluorescence-spectroelectrochemical measurements in CH_2Cl_2. **5** and **6** emit weakly at 466 and 473 nm (**5**, λ_{ex} = 336 nm, ϕ = 0.003; **6**, λ_{ex} = 324 nm, ϕ = 0.027).

Received 16th December 2013,
Accepted 5th February 2014

DOI: 10.1039/c3qi00103b

rsc.li/frontiers-inorganic

Introduction

Oxidation of amine is a significant reaction in biology.[1] In the laboratory, the transition metal promoted oxidative dehydrogenation (OD) reaction of amines has been an area of research since 1960 and the reaction was first reported by Curtis *et al.*[2] To date, several OD reactions mediated by transition metal ions with different mechanistic aspects have been reported.[3] In many cases, participation of the transition metal ions to the $-(2e + 2H^+)$ transfer reaction has been proposed. The accepted mechanism is that the metal ion is oxidized first to a higher oxidation state that will either stepwise oxidize the amine by $1e^-$ transfer *via* a ligand radical intermediate or directly oxidize by $2e^-$ transfer, eliminating protons.[3] It has been reported that the OD reactions of $[Ru(bpy)_2(ampy)]^{2+}$ (ampy = 2-(aminomethyl)pyridine),[4a] $[Ru(tame)_2]^{2+}$ (tame = 1,1,1-tris-

[a]*Department of Chemistry, R. K. Mission Residential College, Narendrapur, Kolkata-700103, India. E-mail: ghosh@pghosh.in; Fax: +91 33 2477 3597; Tel: +91 33 2428 7347*
[b]*Max-Planck Institute for Chemical Energy Conversion, Stiftstr. 34-36, 45470 Mülheim an der Ruhr, Germany*

†Electronic supplementary information (ESI) available: UV-vis/NIR absorption spectra (Fig. S1), cyclic voltammogram of **3** (Fig. S2), X-band EPR spectra of **3** and **4** (Fig. S3), fluorescence spectra of **5** and **6** (Fig. S4), photoactive molecular orbitals (Scheme S1), schematic diagram of the ligand fragmentation considered in MO analyses (Fig. S5), calculated bond lengths of **3**, $\mathbf{3}^+$ and **6** (Table S1), TD DFT calculations (Table S2), population analyses of selected molecular orbitals of **6**, **3**, $\mathbf{3}^+$ (Table S3) and optimized coordinates (Table S4–S6). CCDC 842402, 972492 and 972493. For ESI and crystallographic data in CIF or other electronic format see DOI: 10.1039/c3qi00103b

(aminomethyl)ethane),[4b] $[Ru(en)_3]^{3+}$ (en = ethylenediamine)[4b] $[Ru(sar)]^{2+}$ (sar = sarcophagine, 3,6,10,13,16,19-hexaazabicyclo-(6,6,6)eicosane),[4c] and $[Ru(bpy)_2(NC_5H_4CH(CH_3)OH)]^{2+}$ ($NC_5H_4CH(CH_3)OH$ = 2-(hydroxymethyl)pyridine)[4d] proceed *via* a ruthenium(IV) intermediate. Similarly, intermediacy of M(IV) ions was proposed in the OD reactions of $[Os(bpy)_2(ampy)]^{2+}$,[4e] $[Os(en)_3]^{3+}$ (ref. 4*f*) and $[Fe(sar)]^{3+}$ (ref. 3*a*) complexes. A Ni(III) intermediate also was proposed to participate in the OD reaction of a tetraazamacrocyclic complex of nickel(II) ion.[4g] However, the proposals of the participation of Fe(IV), Ni(III), Os(IV) and Ru(IV) ions in OD reactions are futile.

The reduction of the metal ion during OD reactions has been established only in the cases of copper(II), iron(III) and ruthenium(III) ions by isolating their reduced analogues. Reduction of copper(II) to copper(I) has been established in OD reactions of $[Cu^{II}_2(H_4L)]^{4+}$ (L = octaazamacrocyclic dinucleating ligand),[5a] Cu^{II}(boradiazaindacene (BODIPY) derivative)[5b] and $[Cu^{II}(L)]^{2+}$ (L = *N*,*N*-bis-quinolin-2-ylmethyl-cyclohexane-*trans*-1,2-diamine)[5c] complexes. Reduction of iron(III) to iron(II) in the OD reactions of $[Fe^{III}H_2L]^{3+}$ (H_2L = 1,9-bis(2′-pyridyl)-5-[(ethoxy-2″-pyridyl)methyl]-2,5,8-triazanonane),[5d] tetracyano-(1,2-diamine derivative)ferrate(III)[5e] complexes and formation of a ruthenium(II) analogue in the OD reaction of $[Ru^{III}(O–N)(bpy)_2]^{2+}$ (O–N = unsymmetrical bidentate phenolate type ligand, bpy = 2,2′-bipyridine)[5f] were authenticated. However, the reports of air and base promoted OD reactions of the amine complexes of nickel(II), cobalt(III) and rare earth metal ions are significant.[5g–i]

o-Phenylene diamine derivatives are strong chelating agents and furnished several bioactive transition metal complexes.[6] Thus, the coordination chemistry of *o*-phenylenediamine derivatives is the subject of investigation here. Recently, we reported the OD reaction of a tetradentate *o*-phenylenediamine derivative (L_3H_2) (L_3H_2 = (*E*)-2-(((2-((phenyl(pyridin-2-yl)methyl)-amino)phenyl)imino)methyl)phenol). It was disclosed that the reaction of L_3H_2 with tris(triphenylphosphine)ruthenium(II) precursor results in the OD reaction converting L_3H^- to L_4^-, affording the *trans*-$[Ru(L_4^-)(PPh_3)_2]^+$ (**2**$^+$) cation (L_4H = 2-((*E*)-(2-((*E*)-phenyl (pyridinyl)methyleneamino)phenylimino)methyl)-phenol.[7] However, in the presence of an easily reducible iron(III) ion, no OD reaction occurs and the reaction ends up with the formation of an amine complex, *cis*-$[Fe(L_3H^-)Cl_2]$ (**1**), as shown in Scheme 1.

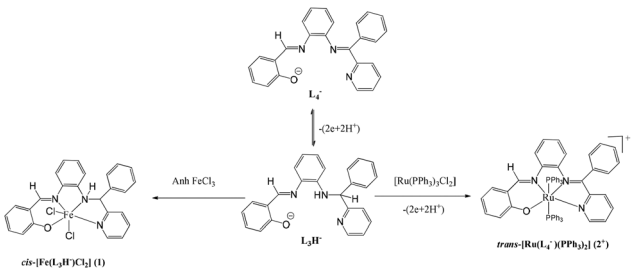

Scheme 1

In this work the role of the metal ions in the OD reaction of the (Ph)(Py)(H)C–N(H)– function of L_3H_2 was further investigated. The question is whether the reaction requires the higher oxidation state of the metal ion to promote the OD reaction acclaimed so far. To explore it, the chemistry of L_3H_2 towards the oxidovanadium(IV) and oxidomolybdenum(VI) ions, which are redox active and participate in electron transfer reaction at lower potential and at neutral pH in several redox-enzymes, has been investigated.[8,9] Further, oxidovanadium(IV) and dioxidomolybdenum(VI) complexes have been reported as effective catalysts for oxo transfer,[10a] epoxidation of olefins,[10b] hydrosilylation of carbonyls[10c] and oxidative bromination[10d] reactions. The reactions of oxidovanadium(IV), oxidomolybdenum(VI) and cobaltous ions with L_3H_2 and $L_3{}^{t\text{-Bu}}H_2$ in air were performed. Surprisingly, the OD reaction does not occur, with oxidizing oxidovanadium(IV) and oxidomolybdenum(VI) ions yielding only the amide products, $[V^{IV}O(L_3{}^{2-})]$ (**3**), $[V^{IV}O\text{-}(L_3{}^{t\text{-Bu }2-})]$ (**4**) and *cis*-$[Mo^{VI}O_2(L_3{}^{2-})]$ (**5**) ($L_3{}^{t\text{-Bu}}H_2$ = (*E*)-2,4-di-*tert*-butyl-6-(((2-((phenyl(pyridin-2-yl)methyl)amino)phenyl)imino)methyl) phenol), while the cobaltous ion promotes the OD reaction, affording a cobalt(III) complex of the ketimine derivative, *trans*-$[Co^{III}(L_4^-)Cl_2]$ (**6**).

The metal ion dependent fluorescence features of the organic chromophore is a significant investigation.[11] It is observed that L_3H_2 is fluorescent due to the internal charge transfer (ICT) from the $\pi_{phenolato}$ to the $\pi_{aldimine}{}^*$ orbital (λ_{ex} = 330; λ_{em} = 470 nm).[7] Lifetimes measurements and time resolved emission spectra (TRES) have confirmed that the lower energy excited state at 390 nm has a higher non-radiative rate constant (k_{nr}). It was noted that due to molecular aggregation at higher concentration, the fluid solution fluorescence spectra of L_3H_2 depend on concentration, which has been investigated by ^{1}H NMR and temperature dependent fluorescence spectra.[7] An interesting observation is that the molecular aggregation of L_3H_2 depends reversibly on temperature. At higher concentration, in addition to the emission band at 470 nm, L_3H_2 displays a lower energy emission band at 525 nm, which disappears upon dilution. It was recorded that **1** has eighty fold stronger emission than L_3H_2 itself, while the ketimine analogue **2**$^+$ ion is non-emissive.[7] The fluid solution fluorescence features of **3**, **4**, **5** and **6** are also recorded at 298 K. It is found that **3** and **4** in fluid solutions at 298 K are non-emissive while the electrogenerated one-electron oxidized analogues, $[V^{V}O(L_3{}^{2-})]^+$ (**3**$^+$) and $[V^{V}O\text{-}(L_3{}^{t\text{-Bu }2-})]^+$ (**4**$^+$) are emissive. The complex **5** is weakly emissive. The fluorescence of L_3H_2 ligand is completely quenched in presence of the reducing cobalt(II) ion, while **6** is brightly emissive.

In this article, to substantiate the role of the metal ions in the OD reaction of L_3H_2, syntheses, spectra and X-ray structures including the diverse fluorescence spectra and the redox series of **3**, **4**, **5** and **6** are reported. Density functional theory (DFT) and time dependent (TD) DFT calculations were performed to elucidate the fluorescent as well as the quenched electronic states of the complexes.

Experimental section

Materials and physical measurements

Reagents or analytical grade materials were obtained from commercial suppliers and used without further purification. $VO(acac)_2$ (acac = acetylacetonate) was prepared by the reported procedure.[10e] Spectroscopic grade solvents were used for spectroscopic and electrochemical measurements. After evaporating MeOH solvents of the sample under high vacuum, elemental analyses and spectral measurements were performed. The C, H and N content of the compounds were obtained using a Perkin-Elmer 2400 series II elemental analyzer. Infrared spectra of the samples were measured from 4000 to 400 cm^{-1} with KBr pellets at room temperature on a Perkin-Elmer Spectrum RX 1 FT-IR spectrophotometer. ^1H NMR spectra in $CDCl_3$ were obtained on a Bruker DPX-300 MHz spectrometer with tetramethylsilane (TMS) as an internal reference. ESI mass spectra were recorded on a micromass Q-TOF mass spectrometer. Electronic absorption spectra in solutions at 298 K were recorded on a Perkin-Elmer Lambda 750 spectrophotometer in the range of 3000–200 nm. Magnetic susceptibility at 298 K was measured on a Sherwood Magnetic Susceptibility Balance. The electroanalytical instrument, BASi Epsilon-EC, for cyclic voltammetric experiments in CH_2Cl_2 solutions containing 0.2 M tetrabutylammoniumhexafluorophosphate as supporting electrolyte was used. A BASi platinum working electrode, platinum auxiliary electrode and Ag/AgCl reference electrode were used for the measurements. The redox potential data are referenced *vs.* the ferrocenium/ferrocene, Fc^+/Fc, couple. In all cases, the experiments were performed with multiple scan rates to analyze the reversibility of the electron transfer waves. BASi Epsilon-EC was used for spectroelectrochemistry measurements. The X-band electron paramagnetic resonance (EPR) spectra were measured on a Magnettech GmbH MiniScope MS400 spectrometer (equipped with temperature controller TC H03), where the microwave frequency was measured with a frequency counter FC400.

The EPR spectra of CH_2Cl_2 solutions of the paramagnetic complexes **3** and **4** were recorded at 298 K. The EPR spectrum of the CH_2Cl_2 frozen glass of **3** at 25 K was also recorded. The fluorescence spectra of the complexes were recorded in CH_2Cl_2 at 298 K. The spectral features of $\mathbf{3}^+$ and $\mathbf{4}^+$ ions were recorded by fluorescence spectro-electrochemical measurements in CH_2Cl_2 solvent at 298 K.

Excitation and emission spectra were recorded using quartz sample tubes in a Perkin Elmer LS 55 luminescence spectrophotometer. The fluorescence quantum yield (ϕ_D) was determined in each case by comparing the corrected emission spectrum of the samples with that of anthracene in MeOH (ϕ_D = 0.20) and CH_2Cl_2 (ϕ_D = 0.30) using the following equation[12] considering the total area under the emission curve.

$$Q = Q_R \frac{F}{F_R} \frac{OD_R}{OD} \frac{n^2}{{n_R}^2} \quad (1)$$

where Q is the quantum yield of the compounds, F is the integrated fluorescence intensity (area under the emission curve), OD is the optical density, and n is the refractive index of the medium. It is assumed that the reference and the unknown samples are excited at the same wavelength. The subscript R refers to the reference fluorophore (anthracene in this case) of known quantum yield. The standard quantum yield value thus obtained is used for the calculation of quantum yields of the systems under various conditions.

Syntheses

(*E*)-2-((2-(Phenyl(pyridin-2-yl)methylamino)phenyl imino)-methyl)phenol (L_3H_2). The compound was prepared by a reported procedure from a zinc complex, $[Zn(L_1)Cl_2]$ (L_1 = (*E*)-N^1-(phenyl(pyridin-2-yl)methylene)benzene-1,2-diamine)).[7]

((*E*)-2,4-Di-*tert*-butyl-6-((2((phenyl(pyridin-2-yl)methyl) amino)-phenyl)imino)methyl)phenol ($L_3{}^{t\text{-Bu}}H_2$). The compound was prepared using $[Zn(L_1)Cl_2]$ as a precursor. To a MeOH solution (25 ml) of $[Zn(L_1)Cl_2]$ (410 mg, 1 mmol), sodium borohydride was added in portions with constant stirring until the reddish orange solution turned light yellow. The solution was evaporated under low pressure and the residue was extracted with diethyl ether. After evaporation of the ether, a yellow oily liquid of L_2H was obtained (L_2H = N^1-(phenyl (pyridin-2-yl)-methyl)benzene-1,2-diamine).[7] To L_2H, MeOH (10 ml) followed by 3,5-di-*tert*-butyl-2-hydroxybenzaldehyde (240 mg, 1 mmol) were added and the resulting solution was refluxed for 30 min and then cooled to 298 K. A yellow crystalline solid of $L_3{}^{t\text{-Bu}}H_2$ separated out and was filtered and dried in air. Yield: 110 mg (60% with respect to 2-benzoyl pyridine). Mass spectral data (ESI, positive ion, CH_3OH): *m*/*z* 492 for $[L_3{}^{t\text{-Bu}}H_2]^+$. ^1H NMR ($CDCl_3$, 300 MHz): δ (ppm) 13.54 (s, 1H), 8.65 (s, 1H), 8.60 (d, 1H), 7.59 (t, 1H), 7.52 (t, 3H), 7.32 (m, 3H), 7.07 (m, 3H), 6.69 (t, 3H), 6.54 (t, 2H) 5.61 (d, 1H), 1.51 (s, 9H), 1.35 (s, 9H). Anal. calcd (%) for $C_{33}H_{37}N_3O$: C, 80.61; H, 7.59; N, 8.55. Found: C, 80.10; H, 7.37; N, 8.42. IR/cm^{-1} (KBr): ν 3370 (vs), 2962 (vs), 1595 (vs), 1508 (vs), 1437 (s), 1330 (s), 1250 (s), 998 (s), 754 (s), 581 (m).

$[V^{IV}O(L_3{}^{2-})]$ (3). To a MeOH solution (30 ml) of L_3H_2 (380 mg, 1 mmol), $VO(acac)_2$ (260 mg, 1 mmol) was added and the resulting solution was heated at 327 K for 10–15 min. The solution was cooled at 298 K and filtered. The filtrate was allowed to evaporate slowly in air. After 2–3 days, a dark brown crystalline compound of **3** separated out, which was filtered and dried in air. Yield: 20 mg (40% with respect to vanadium). Mass spectral data (ESI, positive ion, CH_3OH): *m*/*z* 445 for $[\mathbf{3}]^+$. Anal. calcd (%) for $C_{25}H_{19}N_3O_2V$: C, 67.57; H, 4.31; N, 9.46. Found: C, 65.98; H, 4.15; N, 9.41. IR/cm^{-1} (KBr): ν 3411 (m), 3055 (m), 1604 (vs), 1528 (s), 1464 (vs), 1381 (vs), 1328 (vs), 1202 (m), 1154 (s), 1030 (m), 960 (vs), 844 (m), 739 (vs), 707 (s), 555 (s), 409 (m).

$[V^{IV}O(L_3{}^{t\text{-Bu}\ 2-})]\cdot CH_3OH$ ($\mathbf{4}\cdot CH_3OH$). To a MeOH solution (30 ml) of $L_3{}^{t\text{-Bu}}H_2$ (492 mg, 1 mmol), $VO(acac)_2$ (260 mg, 1 mmol) was added and the resulting solution was heated at 327 K for 10–15 min. The solution was cooled at 298 K and filtered. The filtrate was allowed to evaporate slowly in air. After

2–3 days, a dark brown crystalline compound of **4**·CH_3OH separated out, which was filtered and dried in air. Yield: 23 mg (45% with respect to vanadium). Mass spectral data (ESI, positive ion, CH_3OH): *m*/*z* 557 for $[\mathbf{4}]^+$. Anal. calcd (%) for $C_{33}H_{35}N_3O_2V$: C, 71.21; H, 6.34; N, 7.55. Found: C, 70.18. H, 6.19; N, 7.41. IR/cm^{-1} (KBr): ν 3422 (m), 2949 (s), 1597 (vs), 1477 (vs), 1382 (s), 1326 (vs), 1169 (s), 1031 (m), 954 (vs), 760 (s), 734 (vs), 702 (m), 570 (m).

***cis*-[$Mo^{VI}O_2(L_3^{2-})$] (5).** To a MeOH solution (30 ml) of L_3H_2 (380 mg, 1 mmol), $(NH_4)_2[MoO_4]$ (175 mg, 1 mmol) was added and the resulting solution was heated at 327 K for 60 min. The orange-yellow solid of **5** separated out, which was filtered, dried in air and collected. The product was further re-crystallized by diffusing *n*-hexane to the CH_2Cl_2 solution of the crude product at 298 K for single crystal X-ray structure determination. Yield: 120 mg (~68% with respect to molybdenum). Mass spectral data (ESI, positive ion, CH_3OH): *m*/*z* 507.89 for [**5**]. ^1H NMR ($CDCl_3$, 300 MHz): δ(ppm) 8.66 (s, 1H), 8.34 (d, 1H), 7.79 (t, 1H), 7.61–7.43 (m, 5H), 7.37–7.35 (m, 5H), 7.18–6.91 (m, 4H), 6.37 (s, 1H), 5.30 (s, 1H). Anal. calcd (%) for $C_{25}H_{19}MoN_3O_3$: C, 59.41; H, 3.79; N, 8.31. Found: C, 58.75; H, 3.62; N, 8.15. IR/cm^{-1} (KBr): ν 1614 (vs), 1600 (s), 1547 (s), 1472 (s), 1441 (m), 1384 (m), 1233 (m), 1022 (s), 901 (vs), 915 (vs), 886 (vs), 796 (m), 746 (s), 694 (m), 624 (m).

***trans*-[$Co^{III}(L_4^-)Cl_2$] (6).** To a MeOH solution (30 ml) of L_3H_2 (380 mg, 1 mmol), anhydrous $CoCl_2$ (136 mg, 1 mmol) was added and the resulting solution was heated at 327 K for 60 min. The solution was cooled to 298 K and filtered. The filtrate was allowed to evaporate slowly in air. After 2–3 days, a dark brown crystalline compound of **6** separated out, which was filtered and dried in air. Yield: 90 mg (~66% with respect to cobalt). Mass spectral data (ESI, positive ion, CH_3OH): *m*/*z* 435 for $[\mathbf{6} - 2Cl]^+$. ^1H NMR ($CDCl_3$, 300 MHz): δ(ppm) 10.04 (s, 1H), 8.73 (s, 1H), 8.53 (s, 3H), 7.79 (m, 3H), 7.89–6.16 (m, 10H). Anal. calcd (%) for $C_{25}H_{18}Cl_2CoN_3O$: C, 59.31; H, 3.58; N, 8.30. Found: C, 58.95; H, 3.52; N, 8.15. IR/cm^{-1} (KBr): ν 3422 (s), 1609 (vs), 1528 (s), 1438 (m), 1384 (m), 1350 (m), 1145 (m), 754 (m).

X-Ray crystallographic data collection and refinement of the structures (CCDC 842402 (6), 972492 (4·CH_3OH) and 972493 (5))

Single crystals of **4**·CH_3OH, **5** and **6** were picked up with nylon loops and were mounted on a Bruker AXS Enraf-Nonius Kappa CCD diffractometer equipped with a Mo-target rotating-anode X-ray source and a graphite monochromator (Mo-Kα, λ = 0.71073 Å). **4**·CH_3OH and **5** were measured at 100 K while **6** was measured at 296 K. Final cell constants were obtained from least squares fits of all measured reflections. The intensity data was corrected for absorptions using intensities of redundant reflections. The structures were readily solved by direct methods and subsequent different Fourier techniques. The crystallographic data of **4**·CH_3OH, **5** and **6** are listed in Table 1.

The Siemens SHELXS-97[13a] and SHELXL-97[13b] software packages were used for the solution and the refinement. All non-hydrogen atoms were refined anisotropically. Hydrogen atoms were placed at the calculated positions and refined as riding atoms with isotropic displacement parameters.

Table 1 X-ray crystallographic data for **4**·CH_3OH, **5** and **6**

	4·CH_3OH	**5**	**6**
Formula	$C_{33}H_{35}N_3O_2V$	$C_{25}H_{19}MoN_3O_3$	$C_{25}H_{18}Cl_2CoN_3O$
FW	572.60	505.37	506.21
Cryst. color	Red	Orange	Green
Cryst. syst.	Triclinic	Triclinic	Monoclinic
Space group	$P\bar{1}$	$P\bar{1}$	$P2_1/c$
a (Å)	9.340(3)	7.9292(2)	9.3416(5)
b (Å)	11.616(7)	11.4808(6)	12.8676(7)
c (Å)	13.836(4)	11.7269(9)	19.8225(11)
α (°)	76.22(5)	76.524(4)	90.00
β (°)	83.19(5)	83.276(5)	103.333(3)
γ (°)	88.86(5)	81.837(3)	90.00
V (Å^3)	1447.6(11)	1023.71(10)	2318.5(2)
Z	2	2	4
T (K)	100(2)	100(2)	296(2)
2θ	60.00	62.00	48
Calcd (g cm^{-3})	1.314	1.640	1.450
Reflns collected	18 275	15 702	9921
Unique reflns	8372	6499	3489
Refection $[I > 2\sigma(I)]$	5603	6061	2567
λ (Å)/μ (mm^{-1})	0.71073/ 0.380	0.71073/0.675	0.71073/0.993
F(000)	604	512	1032
R_1[a] $[I > 2\sigma(I)]$/ GOF[b]	0.0682/1.036	0.0263/1.059	0.0432/1.051
R_1[a] (all data)	0.1118	0.0293	0.0609
wR_2[c] $[I > 2\sigma(I)]$	0.1469	0.0675	0.1145
No. of param./ restr.	378/0	289/0	289/0
Residual density (e Å^{-3})	0.852	0.729	0.432

[a] $R_1 = \sum||F_o| - |F_c||/\sum|F_o|$. [b] GOF = $\{\sum[w(F_o^2 - F_c^2)^2]/(n-p)\}^{1/2}$. [c] w$R_2$ = $[\sum[w(F_o^2 - F_c^2)^2]/\sum[w(F_o^2)^2]]^{1/2}$ where w = $1/[\sigma^2(F_o^2) + (aP)^2 + bP]$, $P = (F_o^2 + 2F_c^2)/3$.

Density functional theory (DFT) calculations

All the calculations reported in this article were done with the Gaussian 03W[14] program package supported by GaussView 4.1.

The DFT[15] and TD DFT[16] calculations were performed at the level of the Becke three parameter hybrid functional with the non-local correlation functional of Lee–Yang–Parr (B3LYP).[17] The gas-phase geometries of **3** with doublet spin state, $\mathbf{3}^+$ and **6** with singlet spin state were optimized using Pulay's Direct Inversion[18] in the iterative Subspace (DIIS), 'tight' convergent SCF procedure[19] ignoring symmetry. The optimized coordinates are listed in Tables S8–S11 (ESI†). In all the calculations, a LANL2DZ basis set,[20] along with the corresponding effective core potential (ECP) was used for the metal atom. Valence double zeta with polarization and diffuse functional basis set, 6-31++G**[21] were used for the C, N, O and Cl atoms in all the calculations. For the H atoms, the 6-31G basis set was used.[22] The percentage contributions of the metal, chloride and ligand to the frontier orbital of the optimized geometries were calculated using the GaussSum program

package.[23] The sixty excitation energies on the optimized geometries of **3**, $\mathbf{3}^{+}$ and **6** were calculated by TD DFT[24] calculations.

Results and discussion

The coordination complexes of the amide and imine derivatives of L_3H_2 isolated in this work are depicted in Scheme 2. Details of the syntheses of **3–6** are given in the Experimental section. *o*-Phenylene derivatives are synthesized using the reported procedures.[7] $L_3{}^{t\text{-Bu}}H_2$ and **3–6** are characterized by the elemental analyses and IR, mass, EPR and ^{1}H NMR spectra. The V=O stretching vibrations of **3** and **4** are at 966 and 959 cm^{-1}, while the symmetric and asymmetric stretching vibrations of two *cis* Mo=O[25] resonate at 901 and 915 cm^{-1}. UV/vis absorption spectral data are summarized in Table 2. UV/vis spectra are shown in Fig. S1.† The lower energy absorption bands of **3** and **4** disappear in $\mathbf{3}^{+}$ and $\mathbf{4}^{+}$ ions. Complexes **5** and **6** do not display any lower energy absorption bands.

The paramagnetic **3** and **4** complexes are redox active. The redox series of **3** and **4** were investigated by cyclic voltammetry

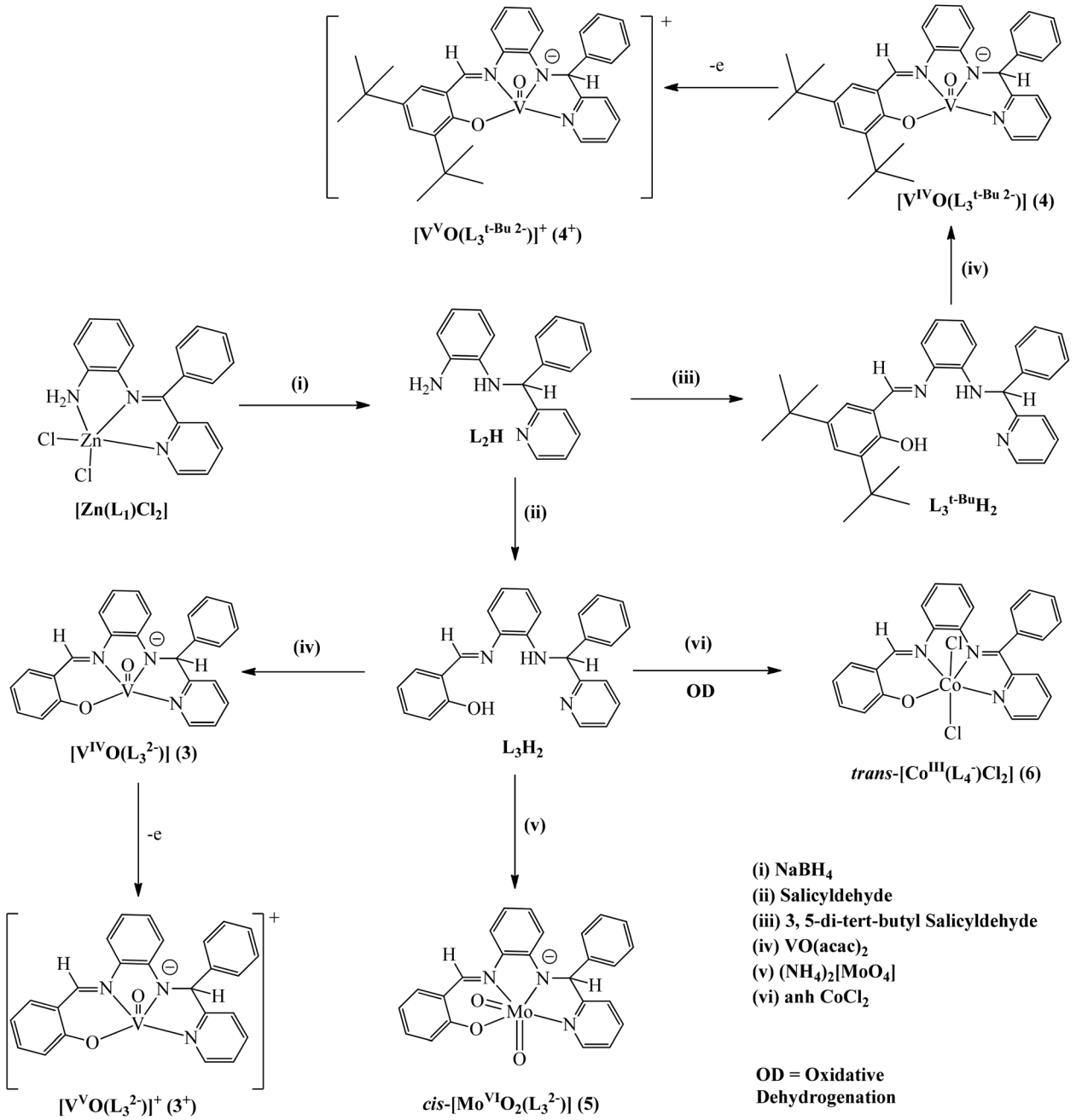

Scheme 2

Table 2 UV-vis/NIR absorption spectral data of **3**, $\mathbf{3}^+$, **4**, $\mathbf{4}^+$, **5** and **6** in CH_2Cl_2 at 298 K

Compound	λ_{max} (ε, 10^4 M^{-1} cm^{-1}) (nm)
3	496 (0.28), 386 (0.44), 327 (0.51)sh, 313 (0.80)sh, 300 (1.24), 266 (1.67)
$\mathbf{3}^+$	491 (0.13)sh, 407 (0.33)sh, 376 (0.49), 331 (0.64)sh
4	492 (0.43), 393 (0.63), 333 (1.72)sh, 316 (2.30)sh, 298 (2.78), 264 (3.20)
$\mathbf{4}^+$	512 (0.13)sh, 421 (0.55), 357 (0.74)sh
5	450 (0.31), 351 (1.01), 326 (1.71)sh 310 (2.23), 256 (2.67)sh
6	423 (0.24), 352 (0.41)sh, 331 (0.53)sh, 303 (0.66), 250 (1.10), 206 (1.74)

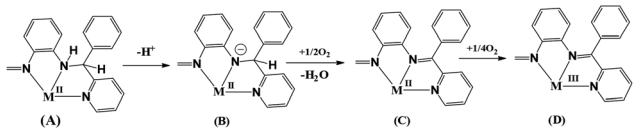

Scheme 3

in CH_2Cl_2 containing 0.2 M tetrabutylammoniumhexafluorophosphate as supporting electrolyte. The cyclic voltammogram of **3** is shown in Fig. S2.† The anodic redox waves of **3** and **4** at 0.35 and 0.33 V are assigned to the VO^{3+}/VO^{2+} redox couple.

No electron transfer occurs in the reactions of L_3H_2 with $VO(acac)_2$ and molybdate ion producing amide complexes **3**, **4** and **5**. However, the reaction of $CoCl_2$ with L_3H_2 affords ketimine complex, **6**. In the reaction with $CoCl_2$, both the metal ion and the ligand undergo oxidation. Overall it is a $-(3e + 2H^+)$ transfer reaction involving an external dioxygen molecule as an oxidizing agent. Scheme 3 illustrates the probable intermediates of this $-(3e + 2H^+)$ transfer redox reaction, which involves: the coordination of the M(II) ion to the monoanionic L_3H^- ligand affording **A**, deprotonation of the monoanionic L_3H^- ligand to the dianionic L_3^{2-} affording **B**, and the oxidation of the dianionic L_3^{2-} to L_4^- by an external oxygen molecule affording **C**. The intermediate **A** has been isolated as a iron(III) complex as **1** (Scheme 1).[7] The intermediate **B** has been isolated as oxidovanadium(IV) and *cis*-dioxidomolybdenum(VI) complexes as **3**, **4** and **5**. In case of ruthenium, **C** is the final product furnishing the $\mathbf{2}^+$ ion (Scheme 1). However, in the case of the cobalt(II) ion, the e_g^1 electron is delocalized over the low-lying $\pi_{diimine}^*$ orbital and reacts easily with air, affording the cobalt(III) complex, **D**.

The OD reaction with the cobalt(II) ion is informative. The higher valent cobalt(IV) ion will never be achieved in air. The conversion of cobalt(II) to cobalt(III) ion in presence of a chelating ligand is easier, however, cobalt(III) ion is not an oxidizing agent. It completely defies the participation of the higher oxidation state of the metal ion in an OD reaction of the amine. One of the important roles of the metal ions is to de-protonate the NH functionality upon coordination, which is achieved in the cases of oxidovanadium and oxidomolybdenum ions. The oxidation occurs *via* the external O_2 molecule facilitating the $d_M \rightarrow \pi_{imine}^*$ back-bonding, which is favored with a t_2^6 state, *e.g.* Ru(II) and Co(III) ions. For effective back-bonding increasing the M–N bond order, it needs a lower oxidation state of the metal ions. Oxidovanadium(IV) and dioxidomolybdenum(VI) ions in **3–5** are, respectively, d^1 and d^0 ions and lack the ability to back donate, significantly disfavoring the OD of the amide ligand.

Molecular geometries

Molecular bond parameters and *cis* or *trans* geometries of **3–6** were confirmed by the single crystal X-ray structure determinations of $\mathbf{4}\cdot CH_3OH$, **5** and **6**. $\mathbf{4}\cdot CH_3OH$ crystallizes in the $P\bar{1}$ space group. The molecular geometry of $\mathbf{4}\cdot CH_3OH$ in the crystals along with the atom labeling scheme is illustrated in Fig. 1. The significant bond parameters are summarized in Table 3. The tetra-dentate $L_3^{t\text{-}Bu\ 2-}$ dianionic ligand spans the sites of the square (with a mean deviation of 0.09 Å) of the distorted square pyramid coordination sphere around the vanadium ion. The vanadium ion is displaced towards the oxido group by 0.65 Å. The oxidovanadium, V(1)–O(40) and the $V(1)–O_{phenolato}$ *i.e.* V(1)–O(1) bond lengths, 1.612(2) and 1.925(2) Å, respectively, correlate well with the presence of the oxidovanadium(IV) ion in $\mathbf{4}\cdot CH_3OH$.[26] The C(8)–N(9) and C(17)–N(16) lengths, 1.303(3) and 1.448(3) Å, respectively, are consistent with the existence of the aldimine, –CH=N– and (Ph)(Py)(H)C–N(H)– functionalities in $\mathbf{4}\cdot CH_3OH$.[7]

5 crystallizes in the $P\bar{1}$ space group. An ORTEP plot of the molecule and the atom labeling scheme are illustrated in Fig. 2. Significant bond parameters are listed in Table 4.

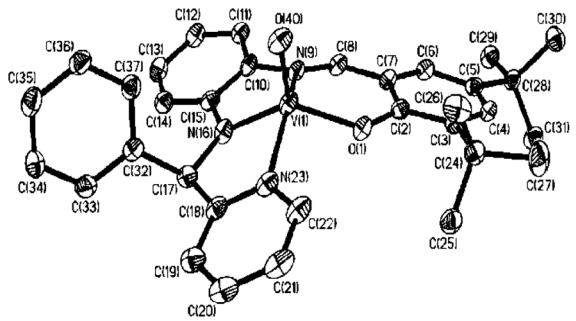

Fig. 1 Molecular geometry of $\mathbf{4}\cdot CH_3OH$ in crystals (50% ellipsoids; CH_3OH and H atoms are omitted for clarity).

Table 3 Selected experimental bond lengths (Å) and angles (°) of $\mathbf{4}\cdot CH_3OH$ and corresponding calculated parameters of **3**

	Exp.	Cal.
	$\mathbf{4}\cdot CH_3OH$	**3**
V(1)–O(1)	1.925(2)	1.923
V(1)–N(9)	2.052(2)	2.066
V(1)–N(16)	1.950(2)	1.968
V(1)–N(23)	2.099(3)	2.110
V(1)–O(40)	1.612(2)	1.599
C(8)–N(9)	1.303(3)	1.302
N(16)–C(17)	1.448(3)	1.448
O(1)–V(1)–N(16)	135.08(9)	133.75
N(9)–V(1)–N(23)	146.09(10)	147.79

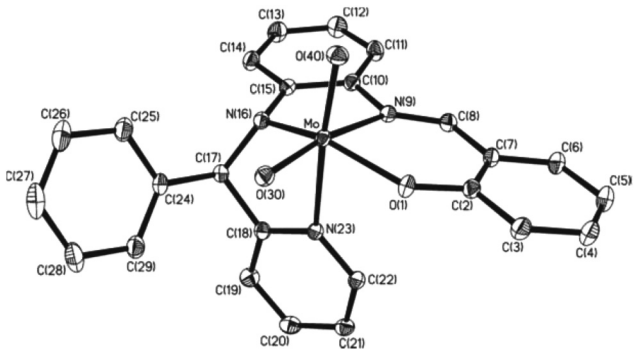

Fig. 2 Molecular geometry of **5** in crystals (50% ellipsoids; H atoms are omitted for clarity).

Table 4 Selected experimental bond lengths (Å) and angles (°) of **5**

Mo–O(1)	1.9692(11)	C(8)–N(9)	1.2934(19)
Mo–N(9)	2.2958(13)	N(16)–C(17)	1.4789(18)
Mo–N(16)	2.0219(12)	O(1)–Mo–N(16)	147.57(5)
Mo–N(23)	2.3637(12)	N(9)–Mo–N(23)	77.79(4)
Mo–O(30)	1.7198(11)	O(40)–Mo–O(30)	107.32(5)
Mo–O(40)	1.7096(11)		

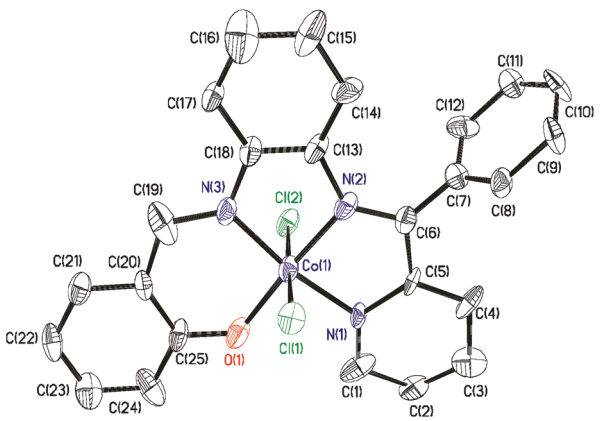

Fig. 3 Molecular geometry of **6** in crystals (50% ellipsoids; H atoms are omitted for clarity).

The orientation of the L_3^{2-} ligand in **5** is different from that in **4**·CH_3OH. The Mo–N_{py} (N(23)) bond is perpendicular to the MoO(1)N(9)N(16) plane, making the two oxido groups *cis* to each other. Two Mo=O bond lengths, 1.7096(11) and 1.7198(11) Å, are similar to those reported in *cis*-dioxidomolybdenum(VI) complexes.[25] The C(8)–N(9) length, 1.294(2) Å, authenticates the aldimine (–CH=N–) functional group, while the C(17)–N(16) length of 1.479(2) correlates well with a C–N single bond.

6 crystallizes in the $P2_1/c$ space group. The molecular geometry of **6** in the crystals and the atom labeling scheme is depicted in Fig. 3. Significant bond parameters are summarized in Table 5. The orientation of the tetra-dentate L_4^- ligand is different from the dianionic $L_3^{t\text{-Bu}\ 2-}$ and L_3^{2-} ligands present in **4**·CH_3OH and **5**. In contrast to the non-planner

Table 5 Selected experimental and calculated bond lengths (Å) and angles (°) of **6**

	Exp.	Cal.
Co(1)–O(1)	1.872(2)	1.888
Co(1)–N(1)	1.933(3)	1.9451
Co(1)–N(2)	1.880(3)	1.916
Co(1)–N(3)	1.870(3)	1.896
Co(1)–Cl(1)	2.2333(10)	2.306
Co(1)–Cl(2)	2.2637(10)	2.306
N(2)–C(6)	1.285(4)	1.299
N(3)–C(19)	1.297(4)	1.306
Cl(1)–Co(1)–Cl(2)	177.55(4)	177.33
O(1)–Co(1)–N(2)	176.30(12)	176.85
N(3)–Co(1)–N(1)	170.08(13)	169.75

Table 6 Significant experimental M–N_{imine}, M–N_{amide} and M–N_{amine} bond lengths (Å)

Bond type	Length	Complexes
Fe^{III}–N_{amine}	2.192(2)	**1**
Ru^{II}–$N_{ketimine}$	1.976(6)	$\mathbf{2}^+$
V^{IV}–N_{amide}	1.950(2)	**4**
Mo^{VI}–N_{amide}	2.022(2)	**5**
Co^{III}–$N_{ketimine}$	1.880(3)	**6**

geometries of $L_3^{t\text{-Bu}\ 2-}$ and L_3^{2-}, the L_4^- in **6** is completely planar, excluding the pendent phenyl groups, and occupies the square plane of the CoN_3OCl_2 octahedron enforcing the two chloride ligands *trans* to each other.

The N(3)–C(19) and N(2)–C(6) lengths, 1.285(4) and 1.297(4) Å, are consistent with the existence of the aldimine (–CH=N–) and ketimine ((Ph)(py)C=N–) functional groups in **6**.[7] The bond parameters and the planarity confirm the –(2e + $2H^+$) oxidation of L_3^{2-} to L_4^- in **6**. The two *trans* Co^{III}–Cl lengths are 2.233(2) and 2.364(2) Å.

The trend of M–$N_{ketimine}$ and M–N_{amine} bond lengths in **1–6** complexes is noteworthy. All three types of bond lengths, M–N_{amine}, M–N_{amide} and M–$N_{ketimine}$, with 3d and 4d metal ions have successfully been determined. The experimental bond lengths are listed in Table 6. It is observed that the M–$N_{ketimine}$ lengths are significantly shorter than the M–N_{amine} and M–N_{amide} lengths. In $\mathbf{2}^+$, the Ru^{II}–$N_{ketimine}$ length, 1.976(6) Å, is intermediate between the reported Ru^{II}–N_{amine} and Ru^{II}=N_{imide} lengths. The average Ru^{II}–N_{amine} and Ru^{II}–$N_{iminoquinone}$ distances in *o*-phenylenediamine complexes are 2.132 and 2.080 Å.[27] The reported average Ru^{II}=N_{imide} length is 1.753 Å.[28] It claims that the bond order of the Ru^{II}–$N_{ketimine}$ in $\mathbf{2}^+$ ion is higher than one. A similar trend has been recorded in the case of Co(III) complex **6** also. The Co^{III}–N_{imine} distance, 1.880(3) Å, is shorter than Fe^{III}–N_{amine} and V^{IV}–N_{amide} distances (Table 6). The observed Co^{III}–$N_{aldimine}$ length in **6** is 1.870(3) Å. In a *o*-phenylenediamine complex, Co^{III}–N_{amine} length is 1.982(8)–2.016(3) Å,[29] while the Co^{III}=N_{imide} length in a cobalt(III) aryl imido complex is 1.675 Å.[30] In **6**, the Co^{III}–$N_{ketimine}$ length being intermediate between the Co^{III}–N single and double bonds corresponds to a

bond order higher than one. The features are explained by the mixing of the d_M–π^* orbitals (*vide infra*) that stabilizes the lower oxidation states of the metal ions and increases the M–$N_{ketimine}$ bond order.

EPR spectra, fluorescence and fluorescence-spectroelectrochemistry

The EPR spectra with simulation are shown in the panels (a–c) of Fig. S3.† The spectra with the hyperfine coupling from ^{51}V nuclei corroborate with $s = 1/2$ spin state and (**3**, $g_{iso} = 1.9806$, $A = 86.9 \times 10^{-4}$ cm^{-1}; **4**, $g_{iso} = 1.9778$, $A = 86.7 \times 10^{-4}$ cm^{-1}) and are consistent with the presence of the oxidovanadium(IV) ion in **3** and **4**. The g values of the axial spectrum (panel (b) of Fig. S3†) of the CH_2Cl_2 frozen glass of **3** at 25 K are: $g_{\|} = 1.9590$, $A_{\|} = 156.4 \times 10^{-4}$ cm^{-1}; $g_{\perp} = 1.9828$, $A_{\perp} = 103.7 \times 10^{-4}$ cm^{-1}. Analysis of the EPR spectra of $\mathbf{3}^+$ and $\mathbf{4}^+$ ions confirms that the oxidation is metal centered, concluding that $\mathbf{3}^+$ and $\mathbf{4}^+$ cations are the oxidovanadium(V) complexes of types $[V^VO(L_3^{2-})]^+$ ($\mathbf{3}^+$) and $[V^VO(L_3^{t\text{-}Bu\ 2-})]^+$ ($\mathbf{4}^+$).

3 and **4** are non-emissive while the oxidized analogues $\mathbf{3}^+$ and $\mathbf{4}^+$ ions are emissive at 298 K. In CH_2Cl_2, **5** and **6** are also fluorescent. The fluorescence data are listed in Table 7 and the relevant spectra are shown in Fig. S4.†

In this regard, it is to be noted that the free L_3H_2 ligand is fluorescent ($\lambda_{ex} = 330$; $\lambda_{em} = 470$ nm) due to the internal charge transfer from the $\pi_{phenolato} \rightarrow \pi_{aldimine}^*$ orbital.[7] **3** and **4** absorb strongly at comparatively longer wavelengths (493 and 497 nm) due to $\pi_{NPh} \rightarrow \pi_{aldimine}^*$ transition and the complexes are non-emissive. However similar to **1**, in $\mathbf{3}^+$ and $\mathbf{4}^+$ ions these lower energy bands are absent and the cations are fluorescent.

It is to be noted that upon oxidation the lower energy absorption bands gradually disappear while fluorescence intensity at $\lambda_{em} = 444$ and 490 nm, respectively, for $\mathbf{3}^+$ and $\mathbf{4}^+$ cations gradually increases as depicted in the panels (b) and (d) of Fig. 4. The spectral features of $\mathbf{3}^+$ and $\mathbf{4}^+$ cations are illustrated in Fig. 4. The lower energy absorption bands of **5** and **6** at 450 and 423 nm are weaker and both the complexes are weakly fluorescent as illustrated in Fig. S4† and Table 7.

The origins of the UV-vis/NIR absorptions of **3–6** were elucidated by the time dependent (TD) density functional theory (DFT) calculations on **3**, $\mathbf{3}^+$ and **6**. The gas phase geometry of **3** was optimized at the B3LYP/DFT level with the doublet spin state while those of $\mathbf{3}^+$ and **6** were optimized with the singlet spin state. Calculated bond parameters are listed in Tables 3, 5 and S1.† The calculated bond parameters are similar to those

Table 7 Fluorescence spectral parameters of the complexes in CH_2Cl_2 at 298 K

Compound	$\lambda_{ex}/\lambda_{em}$ (nm)/ϕ^a
$\mathbf{3}^+$	331/444
$\mathbf{4}^+$	339/490
5	336/466/0.003
6	324/473/0.027

[a] ϕ = quantum yield.

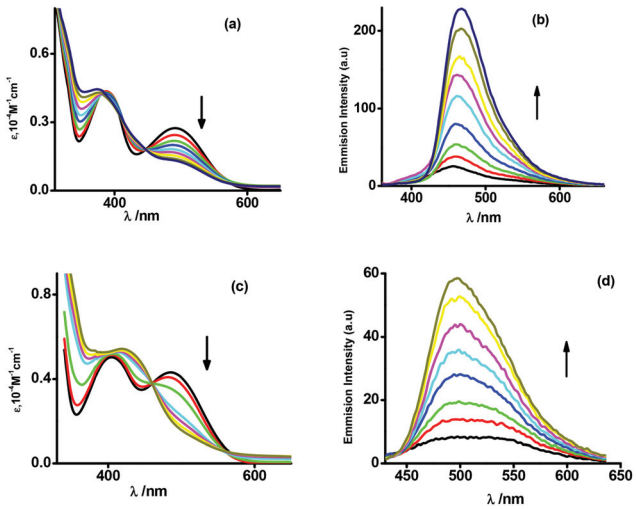

Fig. 4 Spectroelectrochemical measurements of the conversion of **3** → $\mathbf{3}^+$ [(a) UV-vis/NIR absorption and (b) fluorescence spectra] and **4** → $\mathbf{4}^+$ [(c) UV-vis/NIR absorption and (d) fluorescence spectra] in CH_2Cl_2 at 298 K.

obtained from the single crystal X-ray diffraction studies of **4**·CH_3OH and **6** (Tables 3 and 5). The optimized geometries of **3**, $\mathbf{3}^+$ and **6** are shown in Fig. S2.† Excitation energies were calculated by the TD DFT calculations on the optimized geometries. The excitation energies with the oscillator strengths are listed in Table S2.† Fragmentations of the ligand used for the calculations are shown in Fig. S5.† It is reported that L_3H_2 is emissive due to $\pi_{Phenolato} \rightarrow \pi_{aldimine}^*$ transition at $\lambda_{ex} = 330$ nm. **3** and **4** with lower energy absorption bands at $\lambda_{max} = 490$ and 500 nm are non-emissive. The TD DFT calculation on **3** has authenticated that the lower energy absorption band of **3** at $\lambda_{max} = 493.57$ nm with $f = 0.13$ is due to $\pi_{NPh} \rightarrow \pi_{aldimine}^*$ transitions. The $\pi_{phenolato} \rightarrow \pi_{aldimine}^*$ transition of **3** appears at 316.72 nm. However, the non-emissive lower energy absorption band at $\lambda_{max} = 490$ nm gradually disappears upon oxidation of **3** to $\mathbf{3}^+$ (panel (a) of Fig. 4) and $\mathbf{3}^+$ becomes emissive. The calculated excitation band of $\mathbf{3}^+$ at 357.8 nm with $f = 0.12$ is due to $\pi_{phenolato} \rightarrow \pi_{aldimine}^*$ transition. Similarly, the calculated $\pi_{phenolato} \rightarrow \pi_{aldimne}^*$ emissive excitation wavelength of **6** is 318.06 nm ($f = 0.45$). The emissive and non-emissive transitions of **3–6** including the L_3H_2 ligand are illustrated in Scheme S1.†

Molecular orbital analyses

The constituents of the frontier molecular orbitals of **3** and **6** were investigated by DFT calculations using B3LYP functional. Gas phase geometries of **3** and **6** were optimized, respectively, with doublet and singlet spin states. The constituents of the frontier orbitals are analyzed and the data are summarized in Table S3.† The calculations authenticated a significant mixing among the d orbitals and the benzoyl pyridine fragment of the L_4^- ligand in **6**. Analyses have shown that the d_{xz} (HOMO−12) and d_{yz} (HOMO−11) orbitals of the t_2 set of **6** exhibit strong interactions with the benzoyl pyridine fragment of the tetra

dentate diimine ligand. Similar types of mixing among the d orbitals and the L_4^- ligand have been attributed in the case of **3** also. However, the d orbitals of the t_2 set of the OV(IV) ion interact equally with the phenolato and the benzoyl pyridine fragments. The mixing of the d orbitals results in diverse effects in **3** and **6**. In the case of **6**, the d^6 ion promotes the oxidation of amine to ketimine for π delocalization while the d^1 ion stabilizes the hard amide binding in **3**. Similarly, the amide binding is stabilized by the hard acid, d^0, molybdenum (VI) ion. The result is reversed with the soft d^6 ruthenium(II) ion, which converts amine to ketimine for π-delocalization. The OD of the amine to ketimine parallels the chemistry of the conversion of NO → NO^+ reducing metal ions in some cases for effective back-bonding with the lower oxidation states of the metal ions. The results correlate well with the reported conversions of copper(II) to copper(I), d^{10} ion, iron(III) to iron(II) t_2^6 ion and ruthenium(III) to ruthenium(II), t_2^6 ion oxidizing amines to imines.[4]

Conclusion

The role of the oxidation states of the metal ions in oxidative dehydrogenation (OD) reaction of the (Ph)(Py)(H)C–N(H)– functionality of an *o*-phenylenediamine derivative (L_3H_2) has been investigated (L_3H_2 = (*E*)-2-(((2-((phenyl(pyridin-2-yl)-methyl)amino)phenyl)imino)methyl)phenol). Recently, we reported that the reaction of L_3H_2 with anhydrous $FeCl_3$ affords the amine complex *cis*-$[Fe^{III}(L_3H^-)Cl_2]$ (**1**) while the same reaction with $[Ru^{II}(PPh_3)_3Cl_2]$ results in an OD reaction affording a ketimine complex, *trans*-$[Ru^{II}(L_4^-)(PPh_3)]^+$ ($\mathbf{2}^+$), in good yield (L_4H = 2-((*E*)-(2-((*E*)-phenyl(pyridin-2-yl)methyleneamino) phenylimino)methyl)phenol)). To summarize the effect of the higher oxidation states of the metal ions to the OD reaction of L_3H_2, similar reactions of L_3H_2 with oxidovanadium(IV) and oxidomolybdenum(VI) ions were performed. In each case the reaction produces amide complexes of type $[V^{IV}O(L_3^{2-})]$ (**3**), $[V^{IV}O(L_3^{t\text{-}Bu\ 2-})]$ (**4**) and *cis*-$[Mo^{VI}O_2(L_3^{2-})]$ (**5**). However, the reaction of anhydrous $CoCl_2$ with L_3H_2 promotes the OD reaction in air yielding a ketimine complex of type *trans*-$[Co^{III}(L_4^-)Cl_2]$ (**6**). The study infers that the OD reaction of L_3H_2 is not successful with hard metal ions with higher oxidation states, such as Fe^{III}, $V^{IV}O$ and $Mo^{VI}O_4$ ions, while the OD reaction occurs with softer, lower valency Ru(II) and Co(II) ions with the filled t_2^6 set that enhances the $d_M \rightarrow p_\pi^*$ back bonding. The work does not justify the previous reports that claim that the metal ion promoted OD reaction of an amine requires the higher oxidation state as an intermediate for oxidation of amines. The work rather concludes that the coordinated amine is de-protonated to an amide that undergoes oxidation to ketimine by an external oxygen molecule to have stronger $d_M \rightarrow p_\pi^*$ back bonding with the lower oxidation states of the metal ions.

Fluorescence features of L_3H_2 and **3–6** are noteworthy. L_3H_2 is weakly fluorescent (λ_{ex} = 330; λ_{em} = 470 nm) due to a non-emissive lower energy absorption band at 390 nm. **3** and **4** exhibit absorption bands at 493 and 497 nm and are non-emissive, while upon oxidation the lower energy absorption band disappears and $[V^{V}O(L_3^{2-})]^+$ ($\mathbf{3}^+$) and $[V^{V}O(L_3^{t\text{-}Bu\ 2-})]^+$ ($\mathbf{4}^+$) cations are fluorescent, recorded by fluorescence-spectroelectrochemical measurements in CH_2Cl_2 at 298 K. **5** and **6** display weaker absorption bands at 445 and 423 nm and are weakly fluorescent (**5**, λ_{ex} = 336 nm, λ_{em} = 466 nm; **6**, λ_{ex} = 324 nm, λ_{em} = 473 nm). Moreover, in addition to the oxidation state dependent fluorescence features of **3–4**, and oxidovanadium(IV) and dioxidomolybdenum(VI) compounds being effective catalysts for several organic transformations, complexes **3–5** appeared to be significant in coordination chemistry.

Acknowledgements

Financial support received from DST (SR/S1/IC/0026/2012) and CSIR (01/2699/12-EMR-II) New Delhi, India is gratefully acknowledged. SB (CSIR no. 8/531(0006)/2012-EMR-I) and MKB (CSIR no. 8/531(0007)/2012-EMR-I) are thankful to CSIR, New Delhi, India, for fellowships.

Notes and references

1 (*a*) C. Anthony, *Biochem. J.*, 1996, **320**, 697; (*b*) *Metal Ions in Biological Systems*, ed. P. F. Knowles, D. M. Dooley, H. Sigel and A. Sigel, Marcel Dekker, New York, 1994, vol. 30, p. 361; (*c*) M. D. Berry, A. V. Juorio and I. A. Paterson, *Prog. Neurobiol.*, 1994, **42**, 375; (*d*) *Principles and Applications of Quinoproteins*, ed. W. S. McIntire, C. Hartmann and V. L. Davison, Marcel Dekker, New York, 1993, p. 97; (*e*) H. Blaschko, *Rev. Physiol., Biochem. Pharmacol.*, 1974, **70**, 83.

2 (*a*) N. F. Curtis, *J. Chem. Soc. A*, 1971, 2834; (*b*) N. F. Curtis, *Coord. Chem. Rev.*, 1968, **3**, 3; (*c*) N. F. Curtis, Y. M. Curtis and H. K. J. Powell, *J. Chem. Soc. A*, 1966, 1015.

3 (*a*) F. R. Keene, *Coord. Chem. Rev.*, 1999, **187**, 121; (*b*) S. Minakata, Y. Ohshima, A. Takemiya, I. Ryu, M. Komatsu and Y. Ohshiro, *Chem. Lett.*, 1997, **26**, 311; (*c*) A. J. Bailey and B. R. James, *Chem. Commun.*, 1996, 2343; (*d*) P. Muller and D. M. Gilabert, *Tetrahedron*, 1988, **44**, 7171; (*e*) S. I. Murahashi, T. Naota and H. Taki, *J. Chem. Soc., Chem. Commun.*, 1985, 613; (*f*) C. K. Poon and C.-M. Che, *J. Chem. Soc., Dalton Trans.*, 1981, 1019.

4 (*a*) M. J. Ridd and F. R. Keene, *J. Am. Chem. Soc.*, 1981, **103**, 5733; F. R. Keene, M. J. Ridd and M. R. Snow, *J. Am. Chem. Soc.*, 1983, **105**, 7075; (*b*) P. Bernhard, D. J. Bull, H. B. Burgi, P. Osvath, A. Raselli and A. M. Sargeson, *Inorg. Chem.*, 1997, **36**, 2804; B. C. Lane, J. E. Lester and F. Basolo, *Chem. Commun.*, 1971, 1618; D. F. Mahoney and J. K. Beattie, *Inorg. Chem.*, 1973, **12**, 2561; (*c*) P. Bernhard, D. J. Bull, H.-B. Burgi, P. Osvath, A. Raselli and A. M. Sargeson, *Inorg. Chem.*, 1997, **36**, 2804; P. Bernhard and A. M. Sargeson, *J. Chem. Soc., Chem. Commun.*, 1985, 1516; P. Bernhard, A. M. Sargeson and F. C. Anson, *Inorg.*

Chem., 1988, **27**, 2754; P. Bernhard and A. M. Sargeson, *J. Am. Chem. Soc.*, 1989, **111**, 597; P. Bernhard and F. C. Anson, *Inorg. Chem.*, 1989, **28**, 3272; (*d*) M. J. Ridd, D. J. Gakowski, G. E. Sneddon and F. R. Keene, *J. Chem. Soc., Dalton Trans.*, 1992, 1949; (*e*) F. R. Keene, P. A. Lay, G. E. Sneddon and G. W. Whebell, *Aust. J. Chem.*, 1993, **46**, 1763; (*f*) P. A. Lay, A. M. Sargeson, B. W. Skelton and A. H. White, *J. Am. Chem. Soc.*, 1982, **104**, 6161; P. A. Lay and A. M. Sargeson, *Inorg. Chim. Acta*, 1992, **449**, 198; (*g*) P. Maruthamuthu, L. K. Patterson and G. Ferraudi, *Inorg. Chem.*, 1978, **17**, 3157.

5 (*a*) G. J. Christian, A. Llobet and F. Maseras, *Inorg. Chem.*, 2010, **49**, 5977; G. J. Christian, A. Arbuse, X. Fontrodona, M. A. Martinez, A. Llobet and F. Maseras, *Dalton Trans.*, 2009, 6013; (*b*) D. Wang, Y. Shiraishi and T. Hirai, *Chem. Commun.*, 2011, **47**, 2673; (*c*) V. Amendola, L. Fabbrizzi, E. Mundum and P. Pallavicini, *Dalton Trans.*, 2003, 773; (*d*) J. P. Saucedo-Vázquez, V. M. Ugalde-Saldívar, A. R. Toscano, P. M. H. Kroneck and M. E. Sosa-Torres, *Inorg. Chem.*, 2009, **48**, 1214; (*e*) Y. Kuroda, N. Tanaka, M. Goto and T. Sakai, *Inorg. Chem.*, 1978, **17**, 314; (*f*) R. Mitsuhashi, T. Suzuki and Y. Sunatsuki, *Inorg. Chem.*, 2013, **52**, 10183; (*g*) C. L. Weeks, P. Turner, R. R. Fenton and P. A. Lay, *J. Chem. Soc., Dalton Trans.*, 2002, 931; R. K. Wilson and S. Brooker, *Dalton Trans.*, 2013, **42**, 12075; (*h*) A. Panja and P. Guionneau, *Dalton Trans.*, 2013, **42**, 5068; (*i*) Q. Li, S. Zhou, S. Wang, X. Zhu, L. Zhang, Z. Feng, L. Guo, F. Wang and Y. Wei, *Dalton Trans.*, 2013, **42**, 2861.

6 (*a*) N. L. Fry, M. J. Rose, D. L. Rogow, C. Nyitray, M. Kaur and P. K. Mascharak, *Inorg. Chem.*, 2010, **49**, 1487; (*b*) M. J. Rose and P. K. Mascharak, *Inorg. Chem.*, 2009, **48**, 6904; (*c*) M. J. Rose, N. M. Betterley and P. K. Mascharak, *J. Am. Chem. Soc.*, 2009, **131**, 8340; (*d*) G. M. Halpenny and P. K. Mascharak, *Inorg. Chem.*, 2009, **48**, 1490; (*e*) M. J. Rose, C. Nyitray and P. K. Mascharak, *Inorg. Chem.*, 2008, **47**, 11604; (*f*) M. J. Rose, N. L. Fry, R. Marlow, L. Hinck and P. K. Mascharak, *J. Am. Chem. Soc.*, 2008, **130**, 8834.

7 S. Chaudhuri, S. C. Patra, P. Saha, A. Saha Roy, S. Maity, S. Bera, P. S. Sardar, S. Ghosh, T. Weyhermüller and P. Ghosh, *Dalton Trans.*, 2013, **42**, 15028.

8 Vanadium references: (*a*) M. Li, W. Ding, B. Baruah, D. C. Crans and R. J. Wang, *Inorg. Biochem.*, 2008, **102**, 1846; (*b*) D. Rehder, *Bioinorganic Vanadium Chemistry*, John Wiley & Sons Ltd., New York, 2008; (*c*) C. J. Schneider and V. L. Pecoraro, *Vanadium: The Versatile Metal*, ACS Symposium Series 974, American Chemical Society, Washington, DC, 2007, p. 148; (*d*) D. C. Crans, J. J. Smee, E. Gaidamauskas and L. Yang, *Chem. Rev.*, 2004, **104**, 849.

9 Molybdenum references: (*a*) R. Hille, *Dalton Trans.*, 2013, **42**, 3029 and references therein (*b*) Y. Zhang, S. Rump and V. N. Gladyshev, *Coord. Chem. Rev.*, 2011, **255**, 1206; (*c*) R. Hille, *Chem. Rev.*, 1996, **96**, 2757.

10 (*a*) R. Dinda, P. Sengupta, S. Ghosh, H. Mayer-Figge and W. S. Sheldrick, *J. Chem. Soc., Dalton Trans.*, 2002, 4434; C. J. Whiteoak, G. J. P. Britovsek, V. C. Gibson and A. J. P. White, *Dalton Trans.*, 2009, 2337; (*b*) M. A. Katkar, S. N. Rao and H. D. Juneja, *RSC Adv.*, 2012, **2**, 8071; Z. Li, S. Wu, H. Ding, H. Lu, J. Liu, Q. Huo, J. Guan and Q. Kan, *New J. Chem.*, 2013, **37**, 4220; (*c*) P. M. Reis, C. C. Romão and B. Royo, *Dalton Trans.*, 2006, 1842; (*d*) M. R. Maurya, U. Kumarand and P. Manikandan, *Dalton Trans.*, 2006, 3561; (*e*) R. A. Row and M. M. Jones, *Inorg. Synth.*, 1957, **5**, 113.

11 (*a*) H. Xiang, J. Cheng, X. Ma, X. Zhou and J. J. Chruma, *Chem. Soc. Rev.*, 2013, **42**, 6128; (*b*) M. D. Ward, *Coord. Chem. Rev.*, 2010, **254**, 2634; (*c*) *Photofunctional Transition Metal Complexes*, ed. V. W. W. Yam, Springer, Series: Structure and Bonding, 2007, vol. 123; (*d*) M. D. Ward, *Coord. Chem. Rev.*, 2007, **251**, 1663; (*e*) M. Hissler, J. E. McGarrah, W. B. Connick, D. K. Geiger, S. D. Cummings and R. Eisenberg, *Coord. Chem. Rev.*, 2000, **208**, 115.

12 J. R. Lakowicz, *Principles of Fluorescence Spectroscopy*, Springer, 3rd edn, 2006.

13 (*a*) G. M. Sheldrick, *SHELXS97*, Universität Göttingen, Göttingen, Germany, 1997; (*b*) G. M. Sheldrick, *SHELXL97*, Universität Göttingen, Göttingen, Germany, 1997.

14 M. J. Frisch, G. W. Trucks, H. B. Schlegel, G. E. Scuseria, M. A. Robb, J. R. Cheeseman Jr., J. A. Montgomery, T. Vreven, K. N. Kudin, J. C. Burant, J. M. Millam, S. S. Iyengar, J. Tomasi, V. Barone, B. Mennucci, M. Cossi, G. Scalmani, N. Rega, G. A. Petersson, H. Nakatsuji, M. Hada, M. Ehara, K. Toyota, R. Fukuda, J. Hasegawa, M. Ishida, T. Nakajima, Y. Honda, O. Kitao, H. Nakai, M. Klene, X. Li, J. E. Knox, H. P. Hratchian, J. B. Cross, V. Bakken, C. Adamo, J. Jaramillo, R. Gomperts, R. E. Stratmann, O. Yazyev, A. J. Austin, R. Cammi, C. Pomelli, J. W. Ochterski, P. Y. Ayala, K. Morokuma, G. A. Voth, P. Salvador, J. J. Dannenberg, V. G. Zakrzewski, S. Dapprich, A. D. Daniels, M. C. Strain, O. Farkas, D. K. Malick, A. D. Rabuck, K. Raghavachari, J. B. Foresman, J. V. Ortiz, Q. Cui, A. G. Baboul, S. Clifford, J. Cioslowski, B. B. Stefanov, G. Liu, A. Liashenko, P. Piskorz, I. Komaromi, R. L. Martin, D. J. Fox, T. Keith, M. A. Al-Laham, C. Y. Peng, A. Nanayakkara, M. Challacombe, P. M. W. Gill, B. Johnson, W. Chen, M. W. Wong, C. Gonzalez and J. A. Pople, *Gaussian 03, revision E.01*, Gaussian, Inc., Wallingford, CT, 2004.

15 (*a*) *The Challenge of d and f Electrons*, ed. D. R. Salahub and M. C. Zerner, ACS, Washington, D.C., 1989; (*b*) R. G. Parr and W. Yang, *Density Functional Theory of Atoms and Molecules*, Oxford University Press, Oxford, U.K., 1989; (*c*) W. Kohn and L. J. Sham, *Phys. Rev.*, 1965, **140**, A1133; (*d*) P. Hohenberg and W. Kohn, *Phys. Rev.*, 1964, **136**, B864.

16 (*a*) R. E. Stratmann, G. E. Scuseria and M. Frisch, *J. Chem. Phys.*, 1998, **109**, 8218; (*b*) M. E. Casida, C. Jamoroski, K. C. Casida and D. R. Salahub, *J. Chem. Phys.*, 1998, **108**, 4439; (*c*) R. Bauernschmitt and R. Ahlrichs, *Chem. Phys. Lett.*, 1996, **256**, 454.

17 (*a*) A. D. Becke, *J. Chem. Phys.*, 1993, **98**, 5648; (*b*) B. Miehlich, A. Savin, H. Stoll and H. Preuss, *Chem. Phys. Lett.*, 1989, **157**, 200; (*c*) C. Lee, W. Yang and R. G. Parr, *Phys. Rev. B*, 1988, **37**, 785.

18 P. J. Pulay, *J. Comput. Chem.*, 1982, **3**, 556.
19 H. B. Schlegel and J. J. McDouall, *Computational Advances in Organic Chemistry*, ed. C. Ogretir and I. G. Csizmadia, Kluwer Academic, The Netherlands, 1991, p. 167.
20 (*a*) P. J. Hay and W. R. Wadt, *J. Chem. Phys.*, 1985, **82**, 270; (*b*) W. R. Wadt and P. J. Hay, *J. Chem. Phys.*, 1985, **82**, 284; (*c*) P. J. Hay and W. R. Wadt, *J. Chem. Phys.*, 1985, **82**, 299.
21 (*a*) T. Clark, J. Chandrasekhar, G. W. Spitznagel and P. V. R. Schleyer, *J. Comput. Chem.*, 1983, **4**, 294; (*b*) P. C. Hariharan and J. A. Pople, *Theor. Chim. Acta*, 1973, **28**, 213.
22 (*a*) V. A. Rassolov, M. A. Ratner, J. A. Pople, P. C. Redfern and L. A. Curtiss, *J. Comput. Chem.*, 2001, **22**, 976; (*b*) M. M. Francl, W. J. Pietro, W. J. Hehre, J. S. Binkley, D. J. DeFrees, J. A. Pople and M. S. Gordon, *J. Chem. Phys.*, 1982, **77**, 3654; (*c*) P. C. Hariharan and J. A. Pople, *Mol. Phys.*, 1974, **27**, 209; (*d*) P. C. Hariharan and J. A. Pople, *Theor. Chim. Acta*, 1973, **28**, 213; (*e*) W. J. Hehre, R. Ditchfield and J. A. Pople, *J. Chem. Phys.*, 1972, **56**, 2257.
23 N. M. O'Boyle, A. L. Tenderholt and K. M. Langner, *J. Comput. Chem.*, 2008, **29**, 839.
24 (*a*) M. Cossi, N. Rega, G. Scalmani and V. Barone, *J. Comput. Chem.*, 2003, **24**, 669; (*b*) V. Barone and M. Cossi, *J. Phys. Chem. A*, 1998, **102**, 1995.
25 (*a*) J. A. Schachner, P. Traar, C. Sala, M. Melcher, B. N. Harum, A. F. Sax, M. Volpe, F. Belaj and Z. N. C. Mosch, *Inorg. Chem.*, 2012, **51**, 7642; (*b*) Y. L. Wong, L. H. Tong, J. R. Dilworth, D. K. P. Ng and H. K. Lee, *Dalton Trans.*, 2010, **39**, 4602; (*c*) C. Zhang, G. Rheinwald, V. Lozan, B. Wu, P. G. Lassahn, H. Lang and C. Janiak, *Z. Anorg. Allg. Chem.*, 2002, **628**, 1259; (*d*) A. M. Santos, F. E. Kühn, K. B. Jensen, I. Lucas, C. C. Romão and E. Herdtweck, *J. Chem. Soc., Dalton Trans.*, 2001, 1332.
26 (*a*) S. Kundu, S. Maity, T. Weyhermüller and P. Ghosh, *Inorg. Chem.*, 2013, **52**, 7417; (*b*) A. Saha Roy, P. Saha, N. Das Adhikary and P. Ghosh, *Inorg. Chem.*, 2011, **50**, 2488 and references therein.
27 A. Lúci, R. Silva, M. O. Santiago, I. C. N. Diógenes, S. O. Pinheiro, E. E. Castellano, J. Ellena, A. A. Batista, F. B. Do-Nascimento and I. S. Moreira, *Inorg. Chem. Commun.*, 2005, **8**, 1154.
28 R. A. Eikey and M. M. Abu-Omar, *Coord. Chem. Rev.*, 2003, **243**, 83.
29 (*a*) V. Stavila, A. Gulea, S. Shova, Y. A. Simonov, P. Petrenko, J. Lipkowski, F. Riblet and L. Helm, *Inorg. Chim. Acta*, 2004, **357**, 2060; (*b*) Y. Yanase, H. Yoshimura, S. Kinoshita, T. Yamaguchi and H. Wakita, *Acta Crystallogr., Sect. C: Cryst. Struct. Commun.*, 1990, **46**, 36; (*c*) L. P. Battaglia, A. M. Corradi, C. G. Palmieri, M. Nardelli and M. E. V. Tani, *Acta Crystallogr., Sect.B: Struct. Crystallogr. Cryst. Chem.*, 1974, **30**, 1114; (*d*) A. A. Khandar, B. Shaabani, F. Belaj and A. Bakhtiari, *Polyhedron*, 2006, **25**, 1893.
30 X. Hu and K. Meyer, *J. Am. Chem. Soc.*, 2004, **126**, 16322.